Proc. 3rd J-PARC Symposium (J-PARC2019)
JPS Conf. Proc. **33**, 011113 (2021)
https://doi.org/10.7566/JPSCP.33.011113

Study of hard and electromagnetic processes at the CERN SPS: an investigation of the high-μ_{B} region of the QCD phase diagram with NA60+

Gianluca USAI

University of Cagliari and INFN - Italy

E-mail: gianluca.usai@ca.infn.it

(Received January 10, 2020)

The exploration of the phase diagram of Quantum ChromoDynamics (QCD) is carried out by studying ultrarelativistic heavy-ion collisions. The energy range covered by the CERN SPS ($\sqrt{s_{\mathrm{NN}}} \sim 5$–17 GeV) is ideal for the investigation of the region of the phase diagram corresponding to finite baryochemical potential (μ_{B}), and has been little explored up to now. In this paper we describe a new experiment, NA60+, that would address several observables which are fundamental for investigating the possible existence of a first phase transition between hadronic matter and a Quark–Gluon Plasma (QGP) at finite μ_{B}. In particular, we propose to study the production of thermal dimuons in Pb-Pb collisions at different energies, from which one would obtain a caloric curve of the QCD phase diagram that is sensitive to the order of the phase transition. In addition, the measurement of the ρ–$\mathrm{a_1}$ chiral mixing would provide crucial insight into the restoration of the chiral symmetry of QCD. In parallel, studies of heavy quark and quarkonium production would also be carried out, providing sensitivity for transport properties of the QGP and the investigation of the onset of the deconfinement transition. Results of physics performance studies for most observables accessible by NA60+ are discussed, showing that the results of the experiment would lead to a significant advance of our understanding of (non-perturbative) strong interaction physics.

KEYWORDS: Quark-gluon plasma, QCD phase transition, chiral symmetry restoration

1. Exploring the QCD phase diagram at high μ_B with NA60+

QCD has a rich phase structure. While asymptotic freedom allows it to completely define the degrees of freedom in terms of quarks and gluons, hadrons become the relevant degrees of freedom when confinement sets in. The phase diagram, shown in Fig. 1 left, is described in terms of temperature (T) and baryochemical potential (μ_B) . Our knowledge of the QCD phase diagram is largely restricted to the region of low μ_B. Here, lattice QCD ([1] and references therein) provides evidence for a cross-over phase transition at a critical temperature $T_c \sim 155$ MeV (Fig. 1 right). The experiments carried out by colliding (ultra)relativistic heavy ions at the CERN-SPS, BNL-RHIC and CERN-LHC accelerators have so far mostly explored the low μ_{B} region. The results demonstrated that a deconfined state of matter is produced in such collisions, with properties consistent with lattice QCD predictions.
For moderate temperatures and high baryon densities the existence of a first-order phase

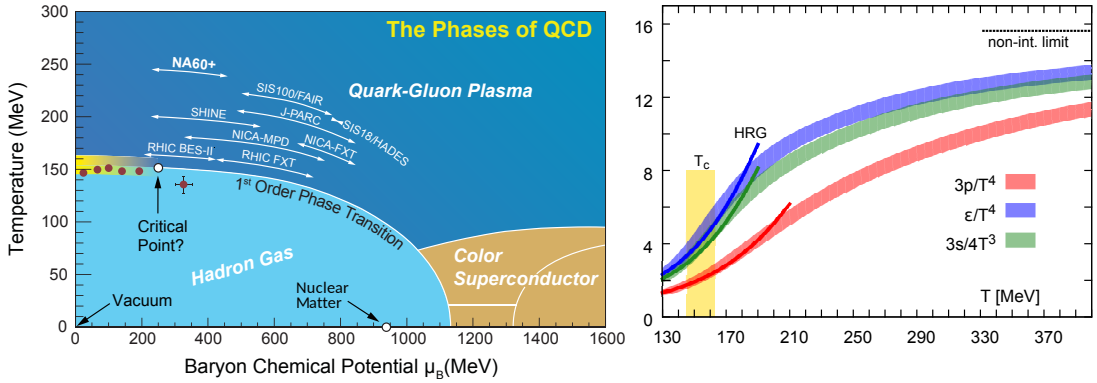

Fig. 1. (Left) The QCD phase diagram (courtesy of Thomas Ullrich). (Right) The temperature dependence of the appropriately scaled energy density (blue), in the limit of vanishing baryon density measured on the lattice [2], is characterized by a rise in the effective number of active degrees of freedom, indicating the cross-over to a QGP.

transition with the co-existence of hadron gas and QGP was suggested by effective field theory calculations [3]. The first-order transition line should end with a second order critical point. Experiments at RHIC (STAR [4]) and the SPS (NA61/SHINE [5]) investigated the phase diagram structure for $\mu_B > 200$ MeV but the existence of such a critical point and the first-order phase transition remain to be confirmed.
The NA60+ physics programme is based on a beam energy scan (BES) in the interval $\sqrt{s_{\rm NN}} \sim$ 6–17 GeV, corresponding to the interval $\mu_{\rm B} = 220 - 440$. It will study dimuon and charm production using the high-intensity lead beams (10^7 ions/s or more) delivered by the CERN SPS. In the following we outline the main physics observables addressed by NA60+ [6].

1.1 thermal dileptons: caloric curve, ρ–a_1 chiral mixing

Evidence for a first-order phase transition between a hadron gas and a QGP can be provided by the measurement of a caloric curve, which relies on precise temperature measurements as a function of the centre-of-mass collision energy. The mass spectrum of thermal dileptons above 1.5 GeV/c^2 provides a precise thermometer of the emitting source with $\mathrm{d}N/\mathrm{d}M \propto M^{3/2} \exp(-M/T_{\rm s})$ [7]. The parameter $T_{\rm s}$ is an average of the temperature T over the fireball evolution, but the high mass range strongly enhances the sensitivity to the early high-T phases of the evolution. Moreover, $T_{\rm s}$ is not affected by the collective motion of the expanding source since mass is a Lorentz-invariant quantity. This method has been exploited by NA60 to measure the medium temperature in In–In collisions at $\sqrt{s_{\rm NN}} = 17.3$ GeV [8, 9].
Chiral symmetry is spontaneously broken in the hadronic world, leading to a mass splitting of $\sim$0.5 GeV/c^2 for the chiral partners ρ–a_1. Lattice QCD for $\mu_B = 0$ shows that chiral symmetry is restored around T_c ([1] and references therein). There is no direct coupling of axial states to the dilepton channel, but in the medium, for dilepton masses above 1 GeV/c^2, 4-π (and higher) states dominate the free electromagnetic correlator. Model-independent predictions of chiral symmetry restoration show that to leading order in temperature one has a pion-induced mixing of vector (V) and axial-vector (A) correlators [10]: $\Pi_V(T) = (1-\epsilon)\Pi_V^{vac} + \epsilon\Pi_A^{vac}$ where ϵ is the mixing parameter ($\epsilon \sim 0.5$ at chiral symmetry restoration). The admixture of the a_1 resonance, via the axial-vector correlator, thus entails an enhancement of the dilepton rate for $M \sim$ 1–1.4 GeV/c^2. Its measurement provides a direct evidence of chiral restoration.

1.2 Open-charm and quarkonia measurements

Heavy-flavour measurements allow fundamental transport coefficients of QCD matter, such as the heavy-quark diffusion coefficient, to be extracted (see e. g. [11]). At finite μ_B, the charm diffusion coefficient is predicted to be larger in the hadronic phase, at temperatures below T_c, than in the QGP phase above T_c [12]. This can be investigated in Pb–Pb collisions at SPS energies, where the hadronic phase $T < T_c$ represents a large part of the space-time evolution of the collisions. Furthermore, measurements of the strange-charm D_s^+ meson and of the Λ_c baryon, compared to the D^0 and D^+ mesons containing only charm and light quarks, are used to characterize the hadronization mechanisms of charm quarks and the role of quark recombination [13]. Finally, the $c\bar{c}$ cross section in hadronic collisions for $\sqrt{s_{NN}} < 17$ GeV was never measured with good precision and, besides providing the optimal normalization for J/ψ production, it is also predicted to be directly sensitive to chiral symmetry restoration.
A suppression of quarkonium states due to colour screening has been considered as one of the key signatures for the formation of a deconfined state [14]. The NA50/60 experiment observed in central Pb–Pb collisions at $\sqrt{s_{NN}} = 17$ GeV an anomalous suppression of the J/ψ production, qualitatively consistent with the melting of the χ_c and $\psi(2S)$ states in the QGP [15, 16]. Quarkonium production in nucleus–nucleus collisions has not been measured below top SPS energy and the possible effects of the formation of a QGP at high μ_B on charmonium states have not been thoroughly investigated by theory. If the observed J/ψ suppression effects are due to the dissociation of the χ_c and $\psi(2S)$ states, one should be able to detect the beam energy threshold for the onset of their suppression. By measuring the corresponding temperature via thermal dimuons, a crucial test of the lattice QCD predictions for the melting temperatures of those charmonium states can be carried out. Furthermore, experimental results about specific effects on various charmonium resonances related to a large μ_B environment may contribute to the characterization of the high-baryon density QGP.

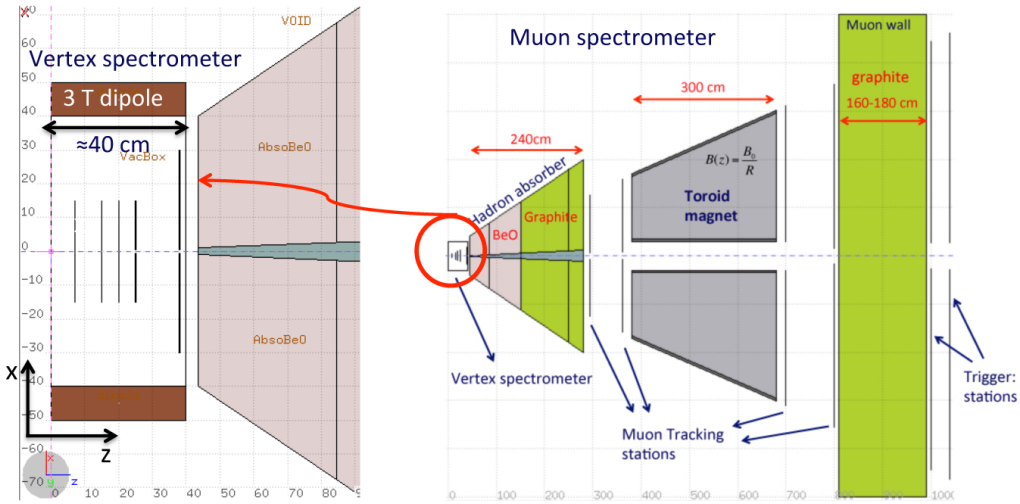

Fig. 2. (Top) Geometry of the proposed experimental apparatus. (Bottom) Perspective view of the main detector subsystems.

2. NA60+: layout and detectors

The NA60+ apparatus is shown in Fig. 2. Muons are measured by a magnetic spectrometer, which is composed of four tracking stations based on GEMs detectors, placed after a hadron absorber. The muon trigger system is downstream of the spectrometer, separated by an additional graphite absorber. A toroidal magnet is placed in between the muon tracking stations and provides a field integral of 0.75 Tm at R=1 m. The absorber allows muons to be identifed, and the distance from the interaction point to the absorber should be small to minimize the background muons from pion and kaon decays. At the same time, the absorber also degrades the kinematics of the muons, because of energy loss fluctuations and multiple scattering. For this reason charged tracks are also measured before the hadron absorber with a silicon vertex tracker (VT) immersed in a 1 Tm dipole field 40 cm long. Muon tracks are matched to the tracks measured by the VT in coordinate and momentum space. In addition, the VT allows the charged-particle multiplicity density and hadronic decays of open-charm particles to be measured.
The silicon spectrometer is also schematically shown in Fig. 2. It consists of 5 silicon tracking planes based on monolithic active pixel sensors (MAPS) in which the sensing volume and readout electronics are in the same silicon wafer. For the NA60+ vertex telescope, the minimization of the multiple scattering due to the material budget and a very good spatial resolution are very important parameters for the muon track matching and for open charm reconstruction.
The apparatus covers the forward rapidity hemisphere, measuring muons in the pseudorapidity interval $1.6 < \eta < 4.5$ and guarantees a good coverage down to low dimuon transverse momenta and rapidity. The set-up will be adapted to the varying beam energy by scaling the absorber thickness and moving the position of the tracking stations so as to keep a good acceptance close to mid-rapidity. More details on the apparatus can be found in [6].

3. Physics performances

In this section the main results of the physics performance studies are presented.

3.1 Thermal dileptons: caloric curve, ρ–a_1 chiral mixing

Studies of thermal radiation were carried out for the 5% most central Pb–Pb collisions at $\sqrt{s_{\rm NN}} = 6.3, 8.8$ and 17.3 GeV. The differential spectra of thermal $\mu^+\mu^-$, $\mathrm{d}^3N/(\mathrm{d}M\mathrm{d}p_{\rm T}\mathrm{d}y)$, are based on the in-medium ρ, ω and 4-pion spectral functions, QGP radiation and the expanding thermal fireball model of [7]. The generator is based on the model calculation which assumes either no ρ–a_1 chiral mixing or full chiral mixing ($\epsilon = 1/2$) in the mass region $1 < M < 1.5$ GeV/c^2. For the performance of the temperature measurement, thermal dileptons were generated without chiral mixing. The hadron cocktail generator for the 2-body decays of η, ω, and ϕ and the Dalitz decays $\eta \to \gamma\mu^+\mu^-$ and $\omega \to \pi^0\mu^+\mu^-$ is based on the NA60 generator and on the statistical model of [17]. The Drell–Yan process and open-charm production are simulated with the PYTHIA event generator.
We present the results for samples of 2×10^7 reconstructed pairs in central collisions at each energy, corresponding to total samples of $\sim 5 \times 10^7$ pairs integrated in centrality. With an SPS beam intensity of 8.5×10^6 lead ions/s, this statistics at a given energy can be collected in a ∼30 days run.
Fig. 3 left shows the net signal at $\sqrt{s_{\rm NN}} = 8.8$ GeV after subtraction of the combi-

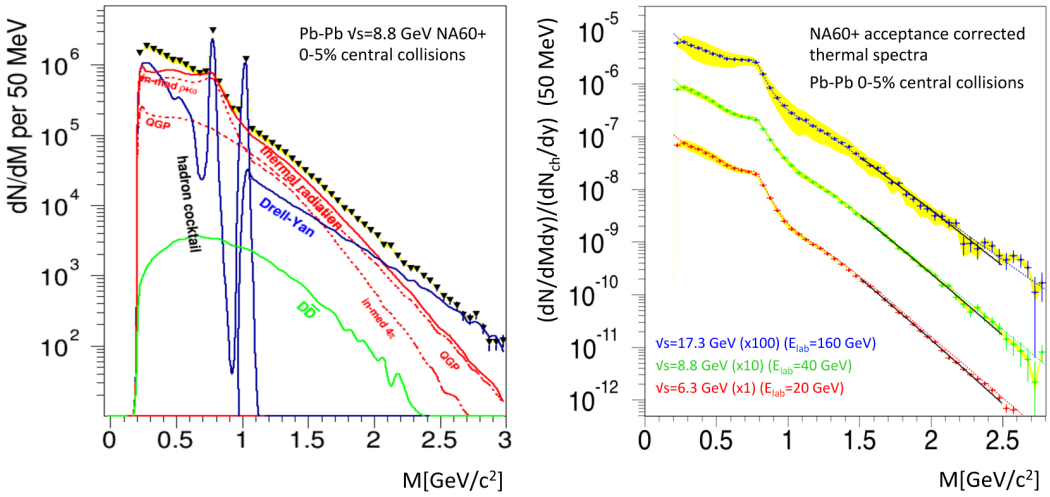

Fig. 3. ((Left) Expected signal sample in the 5% most central Pb–Pb collision at $\sqrt{s_{\rm NN}} = 8.8$ GeV after subtraction of combinatorial and fake matches background. Various contributions are shown (see text for details). (Right) Acceptance corrected thermal spectra at three different beam energies obtained after subtraction of open charm, Drell–Yan and hadronic cocktail. Model comparisons and exponential fits are shown. Systematic uncertainties are shown as yellow band.

natorial background (there is also background arising from incorrect matching of muons with VT tracks - fake matches - but it is rather small, becoming completely negligible for $M > 1$ GeV/c^2). The ω and ϕ peaks are very well resolved with a resolution better than $\sim$10 MeV/c^2 at the ω mass. The figure shows all the expected signal components. The thermal spectra are obtained after (i) subtraction of the hadronic cocktail for $M < 1$ GeV/c^2 of η, ω and ϕ decays into $\mu^+\mu^-$ as well as the η and ω Dalitz decays and (ii) subtraction of Drell–Yan as well as open-charm muon pairs for $M > 1$ GeV/c^2. The open charm becomes totally negligible at low $\sqrt{s_{\rm NN}}$, while the Drell–Yan yield will be measured in dedicated pA runs (see also section 3.2). After acceptance correction, the thermal spectra are fit with $\mathrm{d}N/\mathrm{d}M \propto M^{3/2} \exp(-M/T_s)$ in the interval $M = 1.5$–2.5 GeV/c^2 (Fig. 3 right). The resulting temperatures are compared to the theoretical model used as an input in Fig. 4 left. At low energies, the temperatures can be measured with a combined statistical and systematic uncertainty of just a few MeV, thus showing that the experiment has a strong sensitivity to a possible flattening of the caloric curve in a region complementary to the one which will be explored by CBM, at FAIR.

The acceptance corrected mass spectrum at $\sqrt{s_{\rm NN}} = 8.8$ GeV, based on the assumption of no chiral mixing and in a scenario of small QGP production, is compared to the expectation of full chiral mixing in Fig. 4 right. As shown, the statistical and systematic uncertainty provide a very good sensitivity to an increase of the yield due to chiral mixing of $\sim$20–30%.

3.2 Open-charm and quarkonia measurements

Open-charm hadrons can be fully reconstructed with the NA60+ apparatus via their decays into two or three charged hadrons. In particular, the following decays could enable the measurement of non-strange and strange D mesons as well as Λ_c baryons: $\mathrm{D}^0 \to \mathrm{K}^-\pi^+$, $\mathrm{D}^+ \to \mathrm{K}^-\pi^+\pi^+$, $\mathrm{D}_s^+ \to \phi\pi^+ \to \mathrm{K}^+\mathrm{K}^-\pi^+$, $\Lambda_c^+ \to \mathrm{pK}^-\pi^+$ and their charge conjugates. The decay particles (pions, kaons and protons) are detected by reconstructing their tracks in the

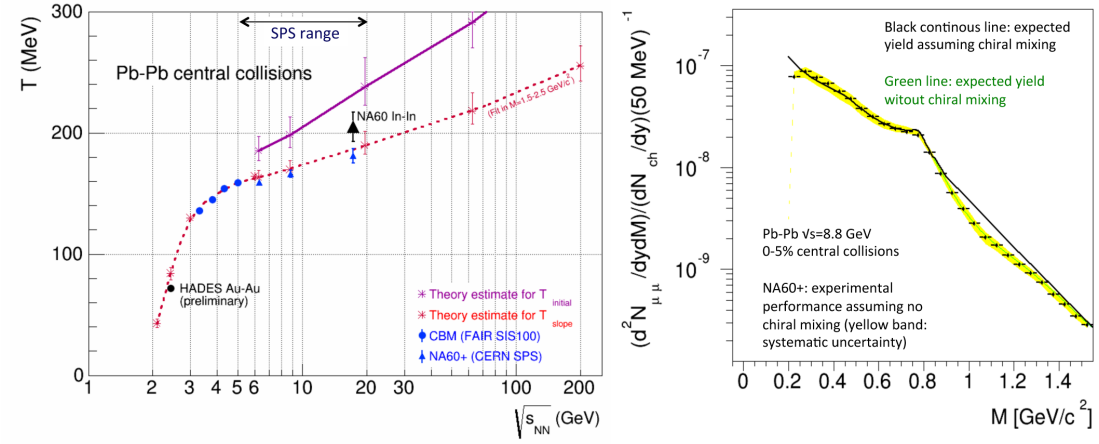

Fig. 4. (Left) Medium temperature evolution vs $\sqrt{s_{\rm NN}}$ in central Pb–Pb collisions. $T_{\rm initial}$ (magenta) and $T_{\rm slope}$ (red) are theoretical estimates for the initial medium temperature and the temperature from dilepton spectra respectively, using Ref. [7] and a coarse graining approach in UrQMD [18]. Blue triangles are the expected performance from NA60+ (CBM performance is also shown [19]). The only existing measurements at present are from NA60 in In–In [8,9] and from HADES in Au–Au collisions [20]. (Right) NA60+ projection for the acceptance corrected thermal dimuon mass spectrum at $\sqrt{s_{\rm NN}} = 8.8$ GeV in case of no chiral mixing compared to the theoretical expectation (green line). The black line above 1 GeV/c^2 is the expectation from full chiral mixing [7].

silicon-pixel detectors of the VT. The huge combinatorial background can be reduced via geometrical selections on the displaced decay-vertex topology, exploiting the fact that the mean proper decay lengths $c\tau$ of open-charm hadrons are of about 60–300 µm, and therefore their decay vertices are typically displaced by a few hundred µm from the primary vertex. Benchmark studies were carried out for the measurement of $\mathrm{D^0} \rightarrow \mathrm{K^-\pi^+}$ in the 5% most central Pb–Pb collisions at two different beam energies: 158 and 60 GeV/nucleon, corresponding to $\sqrt{s_{\rm NN}} = 17.3$ and 10.6 GeV, respectively. The $\mathrm{D^0}$ and $\overline{\mathrm{D^0}}$ mesons were simulated with $p_{\rm T}$ and rapidity distributions obtained with the POWHEG-BOX event generator for the hard-scattering and PYTHIA 6 for the parton shower and hadronization. Fig. 5 left shows a projection for the invariant-mass distribution of $\mathrm{D^0}$ candidates in 5×10^9 central Pb–Pb

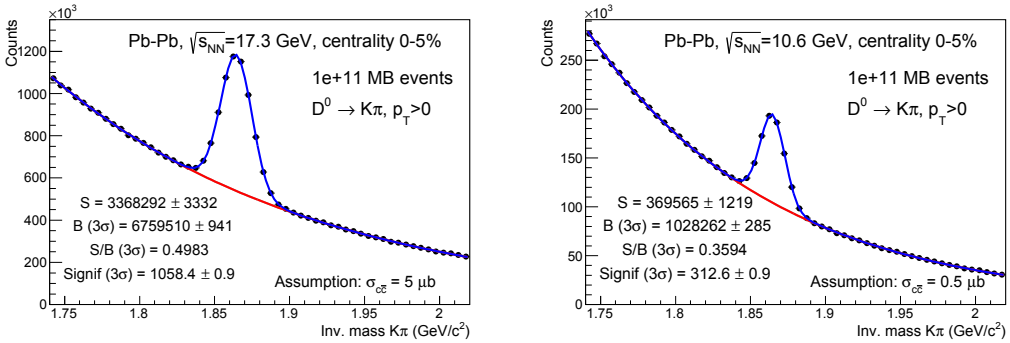

Fig. 5. Projection for invariant-mass distribution of $\mathrm{D^0}$ candidates in 5×10^9 central Pb–Pb collisions at beam energies of 160 (left) and 60 GeV/nucleon (right) for the case of the VT detector based on MAPS with 5 µm spatial resolution.

collisions at $\sqrt{s_{\rm NN}} = 17.3$ GeV, corresponding to a sample of 10^{11} minimum bias (MB) collisions, which can be collected in a few weeks data taking. The MAPS detector would enable a measurement of the D^0-meson yield in central Pb–Pb collisions with a statistical precision much better than 1%, which would allow also for studies in $p_{\rm T}$ and y intervals and for the determination of the elliptic flow coefficient v_2 of D mesons with percent level statistical uncertainty. Fig. 5 right shows the projected performance for the 5% most central Pb–Pb collisions at $\sqrt{s_{\rm NN}} = 10.6$ GeV. For this performance study we assumed $\sigma_{\rm c\bar{c}} = 0.5$ mb and the combinatorial background was simulated based upon the interpolating the NA49 measurements at 40 and 80 GeV/nucleon incident energy. It demonstrates that the integrated D^0-meson cross section can be measured with a statistical precision better than 1% at collision energies at which the charm cross section is poorly known experimentally.

NA60+ proposes to carry out a measurement of J/ψ production approximately down to $\sqrt{s_{\rm NN}} = 8.8$ GeV. At SPS energies, it is well known that the break-up of J/ψ mesons in cold nuclear matter plays an important role in determining the final observed yields in nucleus–nucleus collisions. Therefore, data taking with pA collisions are mandatory to calibrate such an effect. We assumed to have 7 nuclear targets and 15 days of data taking at a beam intensity of 3×10^8 protons/s. Fig. 6 left shows the expected cross sections as a function of the mass number A for $\sqrt{s_{\rm NN}} = 9.8$ GeV ($E_{\rm lab} = 50$ GeV), and assuming a dissociation cross section of $\sigma_{\rm J/\psi–N} = 4.3$ mb. Such measurements are necessary in order to (i) evaluate the J/ψ production cross section $\sigma_{\rm pp\to J/\psi X}$, needed for $R_{\rm AA}$ and (ii) extrapolate break-up effects to the geometrical conditions of Pb–Pb results. These procedures were well tested in past SPS experiments [21]. Fig. 6 right shows the results of a simulation of the J/ψ $R_{\rm AA}$ for

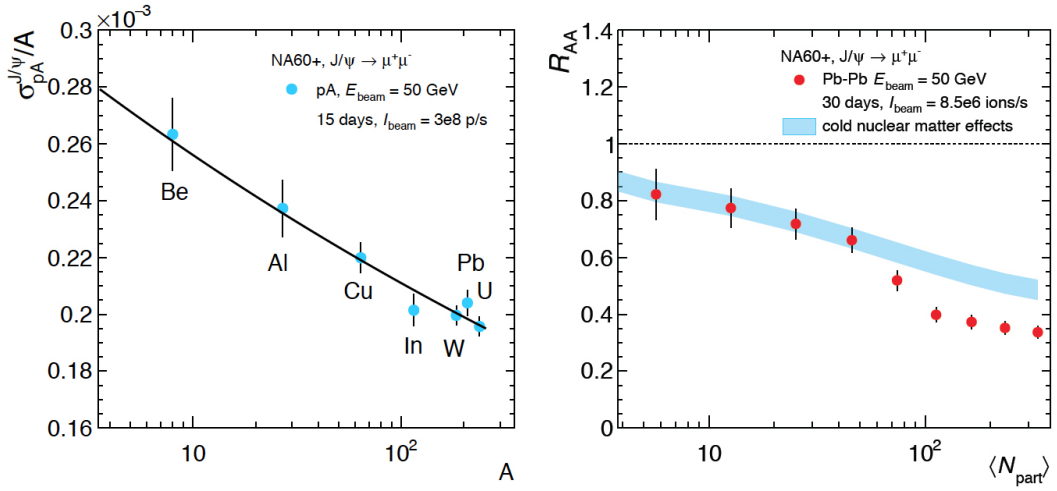

Fig. 6. (Left) J/ψ cross section normalized to the mass number A for pA collisions at $E_{\rm lab} = 50$ GeV. The results of a fit using the parameterisation $\sigma^{\rm J/\psi}_{\rm pA} = \sigma^{\rm J/\psi}_{\rm pp} \cdot A^{\alpha}$ are shown. (Right) The nuclear modification factor for J/ψ production in Pb–Pb collisions at $E_{\rm lab} = 50$ GeV/nucleon as a function of $N_{\rm part}$, compared with expectations from cold nuclear matter effects, obtained from the pA results and shown as a blue band.

Pb–Pb collisions as a function of the number of participant nucleons, $N_{\rm part}$, assuming that for $N_{\rm part} \lesssim 50$ the suppression is entirely due to cold nuclear matter effects, while for more central events an extra-suppression reaching 20% sets in. The simulation assumes 30 days of Pb–Pb collisions at $\sqrt{s_{\rm NN}} = 9.8$ GeV, with an SPS beam intensity of 8.5×10^6 lead ions/s. One can clearly see that a precise evaluation of a relatively small anomalous J/ψ suppression

is within reach down to low $E_{\rm lab}$.

4. Conclusions and outlook

The exploration of the high-$\mu_{\rm B}$ region of the QCD phase diagram represents one of the main directions in the evolution of the field of (ultra)relativistic heavy-ion collisions. This paper discussed the NA60+ project, which aims at performing a comprehensive measurement, in the energy ranged accessible by the CERN SPS, of hard and electromagnetic processes with unprecedented accuracy. The addressed observables include the production of thermal muon pairs, the investigation of the modifications of the vector meson spectral functions as well as the study of charmonia and open charm hadrons. Physics performance studies discussed in this document show that a set-up which makes use of existing advanced detection techniques would be more than enough to carry out the proposed physics programme. An expression of interest was submitted in 2019 to the CERN SPS Council [6], and the submission of a letter of intent is foreseen by the end of 2020.

References

[1] M. D'Elia, Nucl. Phys. A982 (2019) 99, arXiv:1809.10660 [hep-lat].
[2] HotQCD Collaboration, A. Bazavov et al., Phys. Rev. D90 (2014) 094503, arXiv:1407.6387 [hep-lat].
[3] K. Fukushima and T. Hatsuda, Rept. Prog. Phys. 74 (2011) 014001, arXiv:1005.4814 [hep-ph].
[4] STAR Collaboration, L. Adamczyk et al., Phys. Rev. Lett. 112 (2014) 032302, arXiv:1309.5681 [nucl-ex].
[5] NA61/SHINE Collaboration, E. Andronov, Nucl. Phys. A982 (2019) 835, arXiv:1807.10737 [nucl-ex].
[6] NA60+ Collaboration, http://cds.cern.ch/record/2673280.
[7] R. Rapp and H. van Hees, Phys. Lett. B753 (2016) 586.
[8] NA60 Collaboration, R. Arnaldi et al., Eur. Phys. J. C59 (2009) 607, arXiv:0810.3204 [nucl-ex].
[9] NA60 Collaboration, H. J. Specht, AIP Conf. Proc. 1322 (2010) 1, arXiv:1011.0615 [nucl-ex].
[10] M. Dey et al., Phys. Lett. B252 (1990) 620.
[11] A. Beraudo et al., Nucl. Phys. A979 (2018) 21, arXiv:1803.03824 [nucl-th].
[12] F. Scardina, S. K. Das, V. Minissale, S. Plumari, and V. Greco, Phys. Rev. C96 (2017) 044905, arXiv:1707.05452 [nucl-th].
[13] S. Plumari, V. Minissale, S. K. Das, G. Coci, and V. Greco, Eur. Phys. J. C78 (2018) 348, arXiv:1712.00730 [hep-ph].
[14] T. Matsui and H. Satz, Phys. Lett. B178 (1986) 416.
[15] NA50 Collaboration, B. Alessandro et al., Eur. Phys. J. C39 (2005) 335, arXiv:hep-ex/0412036 [hep-ex].
[16] NA60 Collaboration, R. Arnaldi et al., Phys. Rev. Lett. 99 (2007) 132302.
[17] Becattini, F. and Manninen, J. and Gazdzicki, M., Phys. Rev. C73 (2996) 044905, arXiv: hep-ph/0511092 [hep-ph].
[18] S. Endres, H. van Hees, J. Weil, and M. Bleicher, Phys. Rev. C92 (2015) 014911.
[19] T. Galatyuk, Nucl. Phys. A982 (2019) 163.
[20] HADES Collaboration, S. Harabasz et al., Nucl. Phys. A982 (2019) 771.
[21] NA50 Collaboration, B. Alessandro et al., Phys. Lett. B553 (2003) 167.